# Preparation, characterization and adsorption properties of chitosan-iron nanocomposite

Shaimaa A. Hussain

University of Baghdad, College of Education for Pure Science- Ibn Alhaitham, Department of Chemistry, Iraq

Juman A. Naser ( )

University of Baghdad, College of Education for Pure Science- Ibn Alhaitham, Department of Chemistry, Iraq

juman.a.n@ihcoedu.uobaghdad.edu.iq

**Abstract**— Magnetic iron oxide nanoparticles (Fe $_3$ O $_4$ NPs) were prepared using the co-precipitation technique successfully. The prepared nanoparticles were used to modify chitosan (CHT) to use the produced nanocomposite (CHT/ Fe $_3$ O $_4$ NPs) as an adsorbent surface for removing methyl green dye from its aqueous solution .Infrared spectroscopy (FT-IR), scanning electron microscopy (SEM), X-ray dispersion spectroscopy (EDS), X-ray diffraction spectroscopy (XRD) and thermal gravimetric analysis (TGA) were used to characterize (Fe $_3$ O $_4$ NPs) and (CHT/ Fe $_3$ O $_4$ NPs). The system of adsorption was described by Langmuir, Freundlich and Temken models. The adsorbed dye capacity increases with increasing temperature which indicates to the endothermic nature of adsorption.

**Keywords**— Nanocomposite; Iron oxide; Chitosan; Adsorption; Methyl green dye; Isotherm.

#### 1 Introduction

The development of efficient sorbents for water treatment is currently of great interest [1,2]. Several methods have recently been researched for the creation of more economical and effective natural polysaccharide adsorbents [3,4]. The enormous quantity of amino and hydroxyl groups in chitosan and chitin derivatives is of significant importance as an organic component in the composites created for water treatment, as adsorption processe [5–7].

Furthermore, chitosan has the following characteristic: excellent adherence to surfaces, a wide pH stability range, and exhibited chelating abilities. It has been shown to be a good bioadsorbent for several organic pollutants and hazardous ions [7-9].

Dyes from wastewater are often removed by flotation, ultrafiltration, reverse osmosis, chemical oxidation, ion exchange, precipitation, adsorption and other traditional treatment processes [10-12]. With the exception of adsorption, the most of the preferred methods have intrinsic disadvantages such as limited efficiency, the production of large amounts of sludge, and expensive disposal [13]. Because of its effectiveness, adsorption is the most favored treatment method for removing dyes from wastewater [14]. It offers design flexibility, high-quality, reversible treated effluents and regenerable absorbent materials [15]. Activated carbon, silica, alumina, polyaniline, titanium oxides, zinc oxide, manganese oxides and ferric oxide nanoparticles are some of the materials

that are employed to remove dyes from contaminated water by adsorption [16-23]. These adsorbents may be constituted of synthetic or natural substances, including biosorbents and modified biosorbents, chitosan is one of these surfaces [24-26].

This work describes the preparation of the chitosan-iron nanocomposite for their use as a biosorbent. Iron nanoparticles material was obtained by the co-precipitation method using ammonium hydroxide as reduced agent. Adsorption properties of the obtained nanocomposite were studied with respect to methyl green dye, which are common contaminants in industrial waste waters. In addition, the isotherms of methyl green dye adsorption from their aqueous solutions on produced chitosan nanocomposite were investigated.

## 2 Experimental

#### 2.1 Chemicals

All used chemical materials; ferric chloride, ferrous sulfate heptahydrate, ammonium hydroxide, chitosan/ HMW-161.2 and methyl green dye, as shown in (Figure 1) have been purchased from Sigma-Aldrich.

Fig.1. Chemical structure of methyl green dye.

### 2.2 Instruments

Electronic balance/ Sartorius-CPA22, Hotplate stirrer/ LabTech LMS-1003, Oven/ Labtech-LDO-60e, Furnace Oven/ Cole-Parmer WZ-33859-03, Shaking Water Bath/ HYSC- SWB-25, UV/VIS spectrophotometer/ Shimadzu-S8400, FT-IR spectrophotometer/ Shimadzu-1800, Scanning electron microscope/ TESCAN- S8000, X-Ray diffractometer/ Shimadzu-6000, Thermo gravimetric Analyzre/ STA TT-1000.

## 2.3 Preparation of magnetic iron oxide nanoparticles

In this study, magnetic iron oxide nanoparticles (Fe<sub>3</sub>O<sub>4</sub> NPs) were prepared with coprecipitation process [27] by preparing an aqueous ferric chloride solution (FeCl<sub>3</sub>.6H2O) with a concentration of (0.006 M) with a volume of (750 mL) in a (2000 mL) glass beaker. An aqueous ferrous chloride solution (FeCl<sub>2</sub>.4H<sub>2</sub>O) was prepared with a concentration of (0.004 M) and a volume of (750 mL). The second solution was

added to the first solution and the mixture was heated until its temperature reached (60 °C). Then (20 mL) of ammonium hydroxide (30%) was added drop by drop with continuous stirring and maintaining the temperature. After the end of the addition, the resulting solution was left for (30 min) at the same temperature with continuous stirring. The reaction mixture was left to cool down and the resulting precipitate was collected then washed with hot distilled water to remove the base residue. After that, the formed precipitate was dried in an oven at (100 °C) for (90 min). It was calcined in a furnace oven at (500 °C) for (180 min), thus obtaining magnetic nanoparticles.

### 2.4 Preparation of chitosan/iron oxide composite(CHT/ Fe3O4NPs)

(6g) of chitosan was weighed and dissolved in (250 mL) of an aqueous solution acidified in acetic acid (1% v/v) with continuous shaking at (50 °C). To prepare the composite, (0.1 g) of magnetic iron oxide nanoparticles was added to (80 mL) of the chitosan solution previously prepared with continuous shaking to obtain (5%) of chitosan/iron oxide composite. The prepared composite was dried an oven for (120 min) at (100 °C). Thus, the material was ground and use it as a surface adsorbent.

#### 2.5 Adsorption Isotherms

A series of aqueous solutions of methyl green dye were prepared at concentrations (20, 25, 30, 35, 40 mg/L) and (10 mL) of each concentration were placed in a glass flask with a capacity of (50 mL). Add to each flask a mass of (0.01 g) of (CHT/Fe<sub>3</sub>O<sub>4</sub>NPs). After that, the five beakers were placed in a shaking water bath at different temperatures (30, 40, 50 °C) until the equilibrium time was reached, which represented by min (90 min). Finally, the adsorbent surface was separated from the dye solution using a centrifuge, and the absorbance was measured by Uv/Vis spectrophotometer at the greatest wavelength of the dye (617 nm), to calculate the amount of dye adsorbed in (mg/g) unit by the following equation [28];

$$q_e = \frac{(c_o - c_e)V}{m} \tag{1}$$

 $q_e$  is the capacity of adsorption (mg/g),  $C_e$  is the concentration of dye at equilibrium (mg/L),  $C_o$  is the initial concentration of dye (mg/L), m is the mass of adsorbent (g) and V is the volume of dye solution (L).

### 3 Results and discussion

## 3.1 Characterization of chitosan/iron oxide composite (CHT/ Fe<sub>3</sub>O<sub>4</sub>NPs)

### 3.1.1 Fourier-transform infrared spectroscopy (FTIR)

Figure (2, a and b) shows the spectrums of the prepared magnetic iron oxide nanoparticles (Fe<sub>3</sub>O<sub>4</sub>NPs) and chitosan/iron oxide composite (CHT/ Fe<sub>3</sub>O<sub>4</sub>NPs). Where it is observed that a many of beams appear at the frequency of (640 cm<sup>-1</sup>), (698 cm<sup>-1</sup>) and (945 cm<sup>-1</sup>) due to the vibration of the Fe-O bond. As for the chitosan/ magnetic iron oxide composite (Figure 4, b), where we notice the shift of most of the Fe-O absorption sites towards lower frequencies, which indicates an interaction between chitosan and nanoparticles. In addition to the presence of a broad peak at the range of (3100-3500 cm<sup>-1</sup>) indicating the vibration of the polymeric (O-H) hydroxyl group, as well as the emergence of two peaks at (1651 cm<sup>-1</sup>) and (1543 cm<sup>-1</sup>) belonging to the amine groups, where these peaks indicate the presence of various forms of amines due to the degree of deacetylation And the appearance of two peaks at (1080 cm<sup>-1</sup>) and (1029 cm<sup>-1</sup>) due to the vibration of the C-O bond, and the presence of a peak at (2877 cm<sup>-1</sup>) due to =C-H.

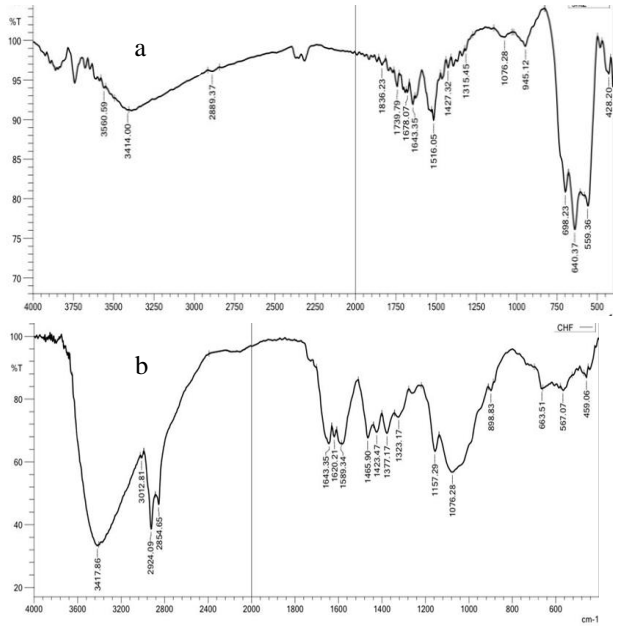


**Fig.2.** FTIR spectrum of a- (Fe<sub>3</sub>O<sub>4</sub>NPs) and b- (CHT/ Fe<sub>3</sub>O<sub>4</sub>NPs).

### 3.1.2 Scanning electron microscope (SEM)

Microscopic images of magnetic iron oxide nanoparticles (Fe<sub>3</sub>O<sub>4</sub>NPs) and chitosan/iron oxide composite using a scanning electron microscope (SEM) were obtained

as shown in Figures (3, a and b) with magnification (200 nm). The microscopic image shows a high attraction between the prepared particles, taking the cubic form with diameters range (20-30 nm). On the other hand, the image of the composite (CTS/Fe $_3$ O $_4$ NPs) shows a close attachment of the particles to the polymer matrix with an increase in their size within the range (30-40 nm), which may be due to the encapsulation of the nanoparticles with chitosan.

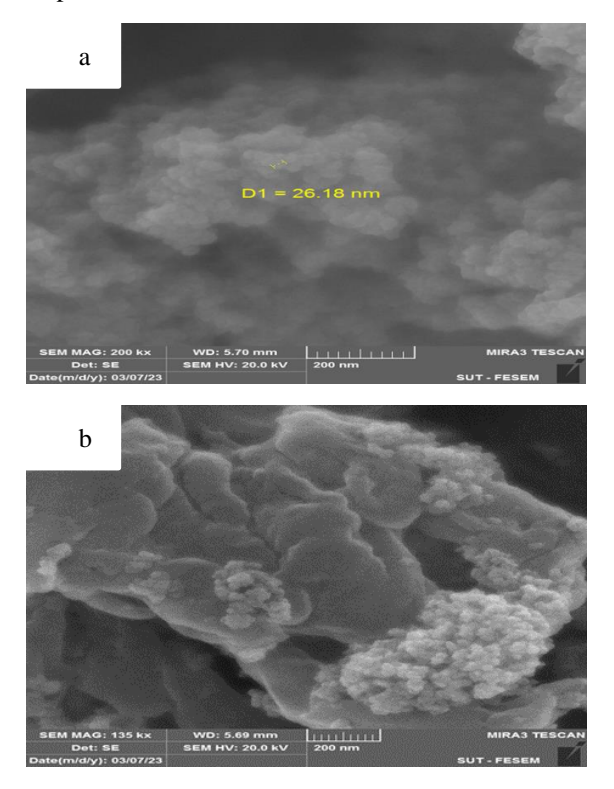


Fig.3. SEM microghraph of a- (Fe<sub>3</sub>O<sub>4</sub>NPs) and b- (CHT/ Fe<sub>3</sub>O<sub>4</sub>NPs).

## 3.1.3 X-ray dispersion spectroscopy (EDS)

X-ray scattering spectroscopy was used to know the chemical properties examined, by determining the proportions of its constituent elements. Figure (4, a and b) shows the EDS spectrum of (Fe $_3$ O $_4$ NPs) and (CTS/Fe $_3$ O $_4$ NPS). It is clear from Figure (4, a) that the atomic percentages were 61.8% and 27.9% for each of iron and oxygen, respectively in the prepared nanoparticles.

In Figure (4, b) the EDS spectrum of the composite (CTS/Fe<sub>3</sub>O<sub>4</sub>NPS), it is noted that the elements iron and oxygen are present in addition to carbon and nitrogen, which are among the components of chitosan, which confirms success of the composite preparation.

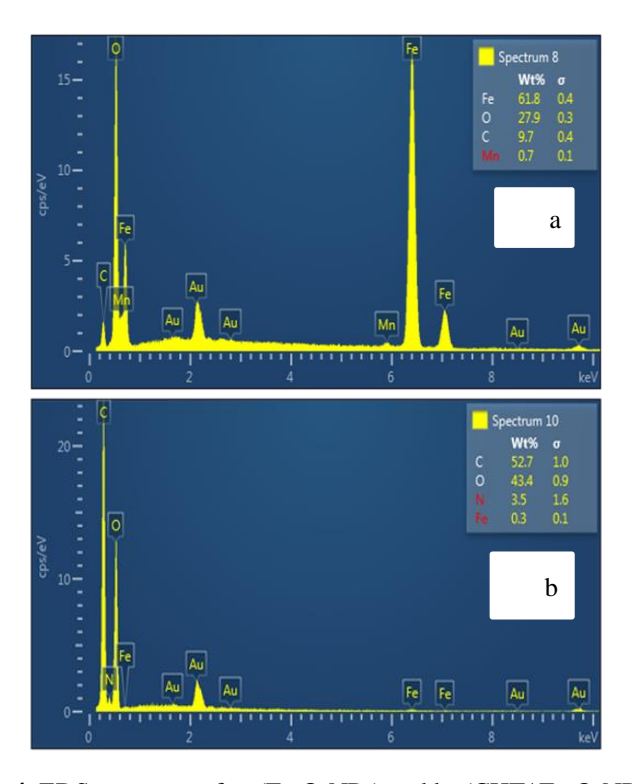


Fig.4. EDS spectrum of a- (Fe $_3$ O $_4$ NPs) and b- (CHT/ Fe $_3$ O $_4$ NPs).

## 3.1.4 X-ray diffraction spectroscopy (XRD)

The crystal structure of (Fe<sub>3</sub>O<sub>4</sub>NPs) and (CTS/Fe<sub>3</sub>O<sub>4</sub>NPs) prepared using X-ray diffraction spectroscopy technique, as in Figure (5, a and b), were investigated. Figure (5, a) shows the diffraction peaks of nanoparticles prepared at  $2\theta$  (31°, 43.5°,36°, 54°, 57.5°,63°) which indicate the cubic shape, and it was found that the average crystal size of the particles is (30 nm), according to the Debye Scherrer equation [29]:

$$D = \frac{0.89 \,\lambda}{\beta \cos \theta} \tag{2}$$

where D is the size of crystallite (nm),  $\lambda$  is the wavelength of x-ray (nm),  $\beta$  is the full width at the half maximum and  $\theta$  is the angle of diffraction.

Figure (5, b) shows the X-ray spectrum of the composite (CTS/Fe<sub>3</sub>O<sub>4</sub>NPs) which indicates that diffraction patterns do not appear for nanoparticles, which is due to the low doping percentage, with the appearance of a simple beam at  $(35^{\circ})$  2 $\theta$ . So, the nanoparticles appeared to be (40 nm).

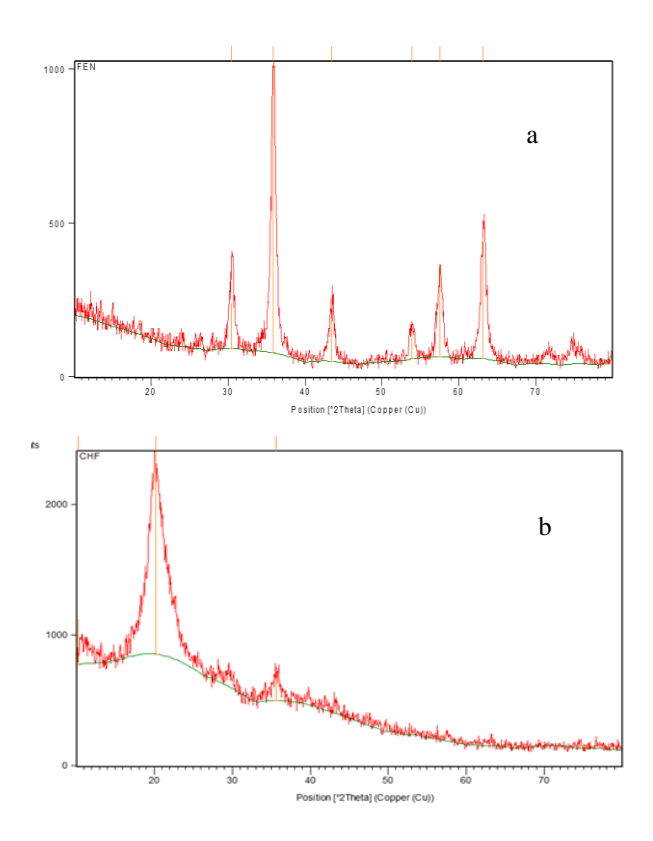


Fig.5. XRD spectrum of a- (Fe<sub>3</sub>O<sub>4</sub>NPs) and b- (CHT/ Fe<sub>3</sub>O<sub>4</sub>NPs).

### 3.1.5 Thermal gravimetric analysis (TGA)

Thermogravimetric analysis (TGA) of chitosan (CTS) and its composite (CTS/Fe<sub>3</sub>O<sub>4</sub>NPs) was carried out by heating them to a temperature of (1000 °C) at a rate of (10° C/min) in an Arcon atmosphere. Figure (6, a and b) shows the loss of chitosan (10.30%) of its weight when heated to (140° C), while the percentage loss is (0.97%) when the heating temperature reaches (250° C). Thus, the weight loss continues until it reaches 54.99% at (450° C), and the final loss percentage is 35.26% at (450° C). On the other hand, Figure (6, b) composite shows an increase in the stability of chitosan compared to what it was before doping, as the loss percentage reached 8.965% of its weight when the heating degree reached (160° C), while at (470° C) the weight loss percentage reached 50.86%. The loss at (980° C) was 31.05%. In general, it was observed that the loss ratio of the composite is less than that of the pure polymer, and this confirms the effectiveness of nanoparticles in improving thermal stability.

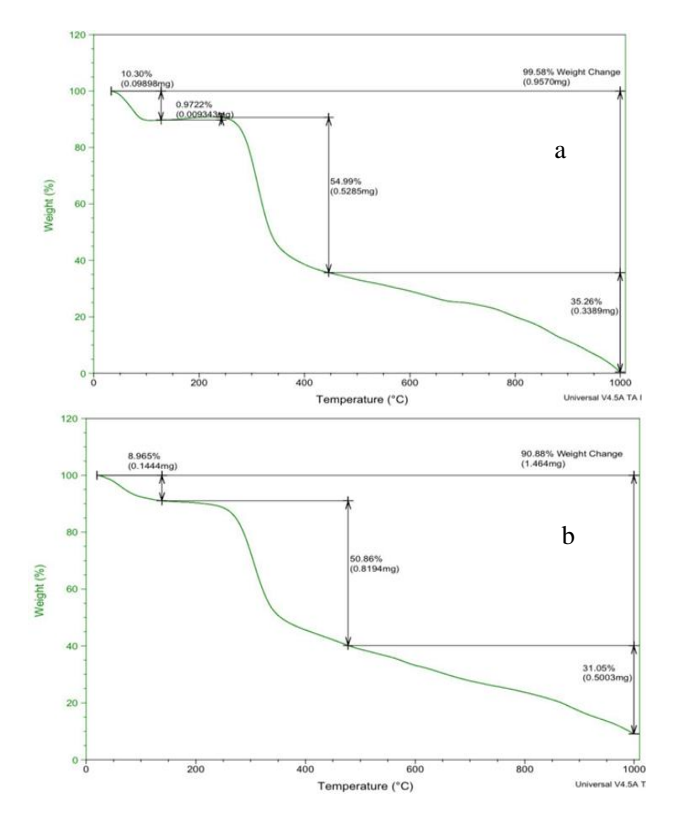


Fig.6. TGA analysis of a- (CHT) and b- (CHT/ Fe<sub>3</sub>O<sub>4</sub>NPs).

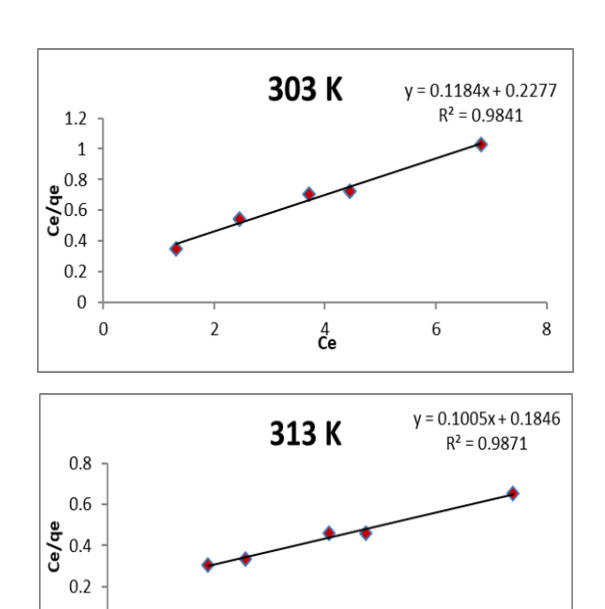
# 3.2 Adsorption Isotherms

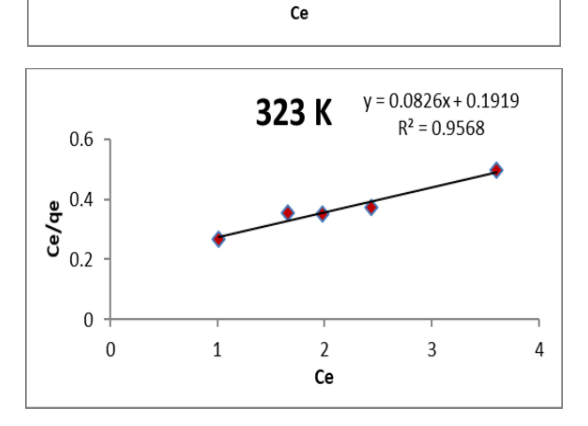
## 3.2.1 Langmuir isotherm

The linear equation of Langmuir model [30] was applied to the practical results of the adsorption experiments of methyl green dye in aqueous solution on the adsorbent surface (CTS/Fe<sub>3</sub>O<sub>4</sub>NPs) at different temperatures (303, 313, 323 K). The values of  $\frac{C_e}{q_e}$  versus  $C_e$  were graphically plotted to find the values of each of  $k_l$ , qmax of the slope and intercept of the straight line equation, respectively, as shown in (Figure 7).

$$\frac{C_e}{q_e} = \frac{1}{q_{max} k_l} + \frac{C_e}{q_{max}} \tag{3}$$

where  $q_e$  is the amount of adsorbed dye at equilibrium (mg/g) and  $C_e$  is the concentration of adsorbed dye at equilibrium (mg/L). Both  $q_{max}$  or  $k_l$  is the experimental constant.





2

3

4

0

1

Fig.7. Diagrams of Langmuir isotherm for adsorption of methyl green dye on the surface of composite (CHT/  $Fe_3O_4NPs$ ) at the temperature range.

Tables (1) show the values of the correlation coefficient ( $R^2$ ) and Langmuir constants  $q_{max}$  and  $K_L$  for the adsorption of methyl green dye from its aqueous solution on the adsorbent surface prepared in this study (Fe<sub>3</sub>O<sub>4</sub>NPs CTS/) in the studied temperature range.

**Table 1.** Experimental constants of Langmuir model for adsorption of methyl green dye on the surface of composite (CHT/ Fe<sub>3</sub>O<sub>4</sub>NPs) at the temperature range.

Temperature (K)	$k_L(mg/kg)$	<b>q</b> max	$\mathbb{R}^2$
303	4.391	8.445	0.984
313	5.417	9.950	0.987

3.211 12.100 0.930
--------------------

When comparing the results in the tables above for the adsorption system according to Langmuir model that was examined, we notice an increase of the  $q_{\text{max}}$  values with the increase in temperature, and the arithmetic average of the value of the correlation coefficient  $R^2$  is (0.963).

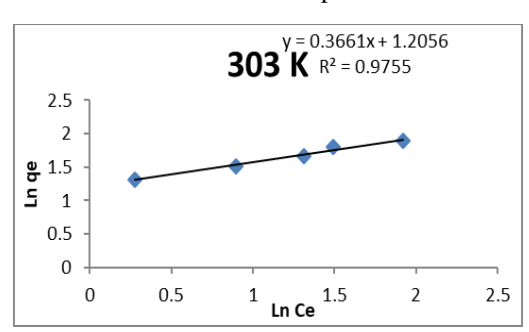
#### 3.2.2 Freundlich isotherm

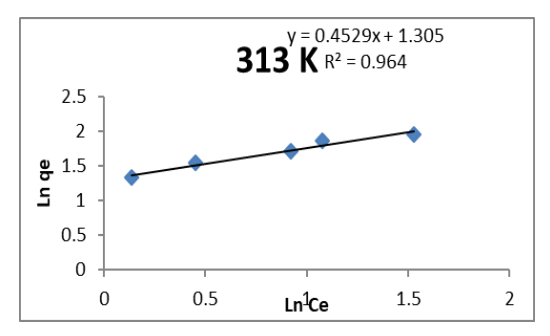
The practical adsorption results of methyl green dye were applied to the studied surface at temperatures (303, 313, 323) K by using the linear equation (4) of Freundlich model [31];

$$\ln q_e = \ln k_f + \frac{1}{n} \ln C_e \tag{4}$$

where  $q_e$  is the amount of adsorbed dye at equilibrium (mg/g) and  $C_e$  is the concentration of adsorbed dye at equilibrium (mg/L). Both  $k_f$  or n is the experimental parameters

Through the graph between the values of  $\ln q_e$  against  $\ln C_e$ , the value of the constant  $k_f$ , which represents the adsorption capacity, is obtained from the intercept value of the straight line equation, while the value of the constant n, which symbolizes the intensity of adsorption is calculated from the slope.





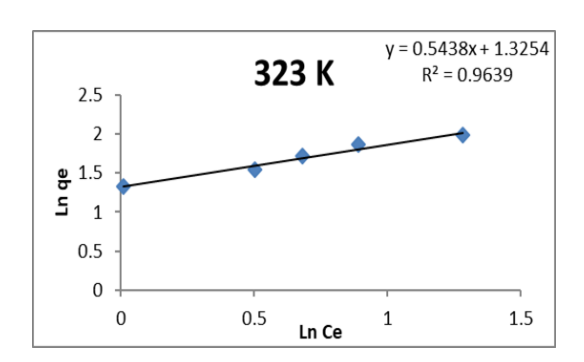


**Fig.8.** Diagrams of Freundlich isotherm for adsorption of methyl green dye on the surface of composite (CHT/ Fe<sub>3</sub>O<sub>4</sub>NPs) at the temperature range.

Tables (2) show the values of Freundlich constants  $k_f$ , n and the correlation coefficient  $R^2$  for the adsorption of methyl green dye from aqueous solution on the surface of composite (CHT/ Fe<sub>3</sub>O<sub>4</sub>NPs) when temperatures under investigation.

**Table.2** Experimental constants of Freundlich model for adsorption of methyl green dye on the surface of composite (CHT/ Fe<sub>3</sub>O<sub>4</sub>NPs) at the temperature range.

Temperature (K)	$k_f$ (mg/kg)	n	$\mathbb{R}^2$
303	3.338	2.731	0.975
313	3.687	2.207	0.964
323	3.763	1.838	0.963

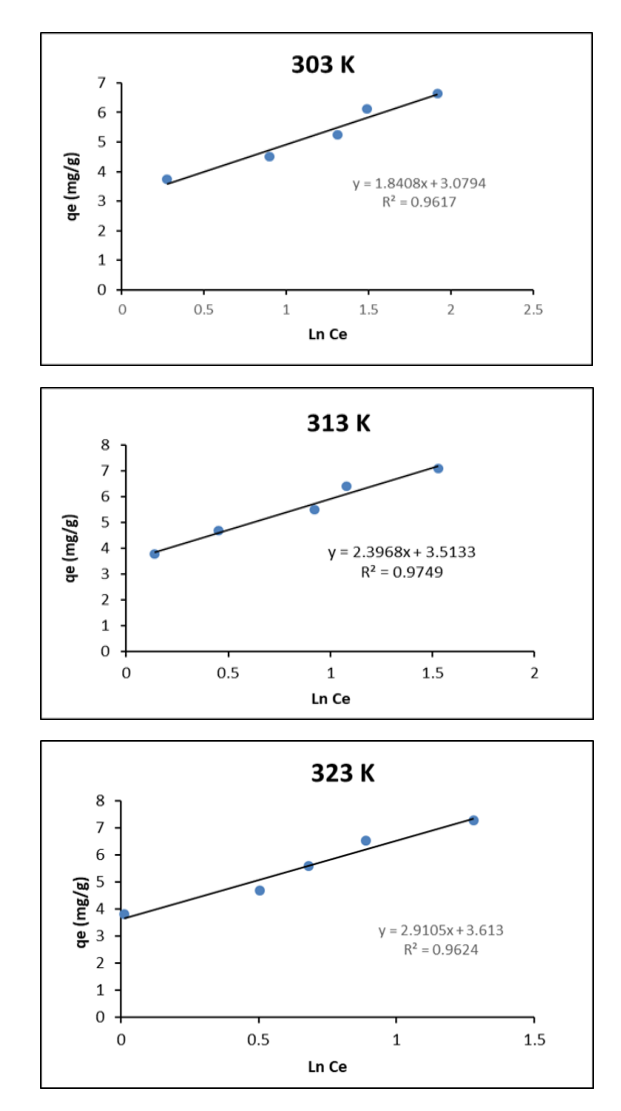
It is noted that the adsorption process is endothermic due to the increase in the value of Freundlich constant (kf) with the increase in temperature by reviewing the data in the above tables. The arithmetic mean of the  $R^2$  values for the studied adsorption system was (0.967).

#### 3.2.3 Temken isotherm

Experimental data were applied for the adsorption of methyl green dye from its aqueous solutions on the prepared composite (CHT/Fe<sub>3</sub>O<sub>4</sub>NPs) as an adsorbent surface at different temperatures (303, 313, 323) K using the linear equation of Temken adsorption model [32]. By plotting the value of  $q_e$  against  $lnC_e$  (Figure 9) the Temken constants  $b_t$  and  $k_t$  were extracted from the slope and cutoff values of the straight line equation graph, respectively.

$$q_e = \ln k_T + b_T \ln C_e \tag{5}$$

where  $q_e$  is the adsorbed dye amount at equilibrium (mg/g),  $b_t$  is the experimental constant and  $C_e$  is the adsorbed dye concentration at equilibrium (mg/L).



 $\label{eq:Fig.9.Diagrams} \textbf{Fig.9.} \ \ \text{Diagrams of Temken isotherm for adsorption of methyl green dye on the surface of composite (CHT/Fe_3O_4NPs) at the temperature range.}$ 

The following table shows the values of Temkin constants  $b_T$ ,  $k_T$  and correlation coefficient  $R^2$  calculated for adsorption of methyl green dye on the surface of (CTS/Fe<sub>3</sub>O<sub>4</sub>NPs) at a range of temperatures.

 $\label{eq:Table 3.} \textbf{Experimental constants of Temken model for adsorption of methyl green dye on the surface of composite (CHT/Fe_3O_4NPs) at the temperature range.}$ 

Temperature (K)	$k_T (L/g)$	$\boldsymbol{b}_T$	$\mathbb{R}^2$
303	5.327	1.840	0.961
313	4.331	2.396	0.974

323	3.460	2.910	0.962
323	5.100	2.710	0.702

It is observed that when the temperature rises kt value decreases  $b_T$  while increases, this indicates that the process of adsorption of methyl green dye increases with the increase in temperature, and the arithmetic average values of the correlation coefficient reached (0.9663).

From all of this, it is concluded that the Langmuir model is the most suitable and compatible with the studied adsorption system.

#### 4 Conclusion

Magnetic iron oxide nanoparticles (Fe<sub>3</sub>O<sub>4</sub>NPs) and its composite (CHT/ Fe<sub>3</sub>O<sub>4</sub>NPs) were prepared effectivelly. Infrared spectroscopy (FT-IR), scanning electron microscopy (SEM), X-ray dispersion spectroscopy (EDS), X-ray diffraction (XRD) and thermal gravimetric analysis (TGA) were utilized to characterize (Fe<sub>3</sub>O<sub>4</sub>NPs) and (CHT/ Fe<sub>3</sub>O<sub>4</sub>NPs). The nanocomposite was used as adsorbent surfaces to adsorb methyl green dye from their aqueous solution at different temperatures. The adsorption isotherms described by Freundlich, Langmuir and Temken models. It was founded that Langmuir model is most suitable to describe the adsorption isotherm.

## 5 References

- 1- Kotyakova, K. Y., Antipina, L. Y., Sorokin, P. B., & Shtansky, D. V. (2022). Efficient and Reusable Sorbents Based on Nanostructured BN Coatings for Water Treatment from Antibiotics. International Journal of Molecular Sciences, 23(24), 16097.
- 2- Naser, J. A., Ahmed, Z. W., & Ali, E. H. (2021). Nanomaterials usage as adsorbents for the pollutants removal from wastewater; a review. Materials Today: Proceedings, 42, 2590-2595.
- 3- Toledo, P. V., & Petri, D. F. (2022). Polysaccharide-Composites Materials as Adsorbents for Organic Dyes. In Textile Wastewater Treatment: Sustainable Bio-nano Materials and Macromolecules, Volume 1 (pp. 185-238). Singapore: Springer Nature Singapore.
- 4- Zhang, W., Xu, Y., Mu, X., Li, S., Liu, X., & Lei, Z. (2023). Research Progress of Polysaccharide-Based Natural Polymer Hydrogels in Water Purification. Gels, 9(3), 249
- 5- Politaeva, N., Yakovlev, A., Yakovleva, E., Chelysheva, V., Tarantseva, K., Efremova, S., ... & Ilyashenko, S. (2022). Graphene oxide-chitosan composites for water treatment from copper cations. Water, 14(9), 1430.
- 6- Bhatt, P., Joshi, S., Bayram, G. M. U., Khati, P., & Simsek, H. (2023). Developments and application of chitosan-based adsorbents for wastewater treatments. Environmental Research, 226, 115530.
- 7- Biswas, S., Fatema, J., Debnath, T., & Rashid, T. U. (2021). Chitosan-clay composites for wastewater treatment: a state-of-the-art review. ACS ES&T Water, 1(5), 1055-1085.

- 8- Piekarska, K., Sikora, M., Owczarek, M., Jóźwik-Pruska, J., & Wiśniewska-Wrona, M. (2023). Chitin and Chitosan as Polymers of the Future—Obtaining, Modification, Life Cycle Assessment and Main Directions of Application. Polymers, 15(4), 793.
- 9- Verma, M., Lee, I., Hong, Y., Kumar, V., & Kim, H. (2022). Multifunctional β-Cyclodextrin-EDTA-Chitosan polymer adsorbent synthesis for simultaneous removal of heavy metals and organic dyes from wastewater. Environmental Pollution, 292, 118447.
- 10- Ahmed, M., Mavukkandy, M. O., Giwa, A., Elektorowicz, M., Katsou, E., Khelifi, O., ... & Hasan, S. W. (2022). Recent developments in hazardous pollutants removal from wastewater and water reuse within a circular economy. NPJ Clean Water, 5(1), 12.
- 11- Anekwe, I. M. S., Adedeji, J., Akpasi, S. O., & Kiambi, S. L. (2022). Available Technologies for Wastewater Treatment. Wastewater Treatment, 33.
- 12- Vidu, R., Matei, E., Predescu, A. M., Alhalaili, B., Pantilimon, C., Tarcea, C., & Predescu, C. (2020). Removal of heavy metals from wastewaters: A challenge from current treatment methods to nanotechnology applications. Toxics, 8(4), 101.
- 13- Al-Mammar, D. E., & Mohammed, R. A. (2017). Application of surfactant for enhancing the adsorption of azo dye onto buckthorn tree wood surface. Iraqi Journal of Science, 1780-1798.
- 14- Jadoo, S. A., & Naser, J. A. (2019). Adsorption thermodynamic study of Congo red dye on electrospun nanofibers mat of polyacrylonitrile. Journal of Global Pharma Technology, 11(7), 401-411.
- 15- Jadoo, S. A., & Naser, J. A. (2020, November). Adsorption optimization of Congo red dye onto electrospun nanofibers of polyacrylonitrile functionalized with Fe3O4 nanoparticles. In IOP Conference Series: Materials Science and Engineering (Vol. 928, No. 5, p. 052024). IOP Publishing.Adeola, A. O., & Nomngongo, P. N. (2022). Advanced polymeric nanocomposites for water treatment applications: A holistic perspective. Polymers, 14(12), 2462.
- 16- Vegas-Mendoza, S. M., Gutierrez-Ortega, J. A., Moran-Salazar, R. G., Cortes-Llamas, S. A., Carbajal-Arizaga, G. G., Peregrina-Lucano, A. A., ... & Gómez-Salazar, S. (2022). L-Glutathione-Functionalized Silica Adsorbent for the Removal of Pesticide Malathion from Aqueous Solutions. Processes, 10(10), 2146.
- 17- Asim, T., Mamoona, Tahir, A., Nisar, N., Ali, A., & Sheikh, A. (2019). Alumina as environmentally stable adsorbent for the removal of diresul black dye from waste water. Water Practice & Technology, 14(1), 62-70.
- 18- Jiang, Y., Liu, Z., Zeng, G., Liu, Y., Shao, B., Li, Z., ... & He, Q. (2018). Polyaniline-based adsorbents for removal of hexavalent chromium from aqueous solution: a mini review. Environmental Science and Pollution Research, 25, 6158-6174.
- 19- Rozman, U., Klun, B., Marolt, G., Imperl, J., & Kalčíková, G. (2023). A study of the adsorption of titanium dioxide and zinc oxide nanoparticles on polyethylene microplastics and their desorption in aquatic media. Science of The Total Environment, 888, 164163.
- 20- Gu, M., Hao, L., Wang, Y., Li, X., Chen, Y., Li, W., & Jiang, L. (2020). The selective heavy metal ions adsorption of zinc oxide nanoparticles from dental wastewater. Chemical Physics, 534, 110750.
- 21- Zhang, L., Wang, J., Qiao, H., Liu, F., & Fu, Z. (2020). Synthesis of manganese oxides for adsorptive removal of ammonia nitrogen from aqueous solutions. Journal of Cleaner Production, 272, 123055.
- 22- Jabbar, K. Q., Barzinjy, A. A., & Hamad, S. M. (2022). Iron oxide nanoparticles: Preparation methods, functions, adsorption and coagulation/flocculation in wastewater treatment. Environmental Nanotechnology, Monitoring & Management, 17, 100661.
- 23- Okoro, H. K., Pandey, S., Ogunkunle, C. O., Ngila, C. J., Zvinowanda, C., Jimoh, I., ... & Adeniyi, A. G. (2022). Nanomaterial-based biosorbents: Adsorbent for efficient

- removal of selected organic pollutants from industrial wastewater. Emerging Contaminants, 8, 46-58.
- 24- Anastopoulos, I., Bhatnagar, A., Bikiaris, D. N., & Kyzas, G. Z. (2017). Chitin adsorbents for toxic metals: a review. International journal of molecular sciences, 18(1), 114.
- 25- Salman, T. A., & Ali, M. I. (2016). Potential application of natural and modified orange peel as an eco-friendly adsorbent for methylene blue dye. Iraqi Journal of Science, 57(1A), 1-13.
- 26- Sumaila, A., Ndamitso, M. M., Iyaka, Y. A., Abdulkareem, A. S., Tijani, J. O., & Idris, M. O. (2020). Extraction and characterization of chitosan from crab shells: kinetic and thermodynamic studies of arsenic and copper adsorption from electroplating wastewater. Iraqi Journal of Science, 2156-2171.
- 27- Naser, J. A. (2016). Electrical properties of liquid crystalline compounds doped with ferric oxide nanoparticles Fe3O4. Int. J. Appl. Chem, 12, 499-511.
- 28- Nandiyanto, A. B. D., Hofifah, S. N., Inayah, H. T., Putri, S. R., Apriliani, S. S., Anggraeni, S., ... & Rahmat, A. (2021). Adsorption isotherm of carbon microparticles prepared from pumpkin (Cucurbita maxima) seeds for dye removal. Iraqi Journal of Science, 1404-1414.
- 29- Holzwarth, U., & Gibson, N. (2011). The Scherrer equation versus the Debye-Scherrer equation'. Nature nanotechnology, 6(9), 534-534.
- 30- Chung, H. K., Kim, W. H., Park, J., Cho, J., Jeong, T. Y., & Park, P. K. (2015). Application of Langmuir and Freundlich isotherms to predict adsorbate removal efficiency or required amount of adsorbent. Journal of Industrial and Engineering Chemistry, 28, 241-246.
- 31- Skopp, J. (2009). Derivation of the Freundlich adsorption isotherm from kinetics. Journal of chemical education, 86(11), 1341.
- 32- Chu, K. H. (2021). Revisiting the Temkin isotherm: Dimensional inconsistency and approximate forms. Industrial & Engineering Chemistry Research, 60(35), 13140-13147.

Article submitted 1 July 2023. Accepted at 17 August 2023. Published at 30 September 2023.